

Optimizing the Principal Eigenvalue of the Laplacian in a Sphere with Interior Traps

A. F. CHEVIAKOV and M. J. WARD

Alexei F. Cheviakov, Department of Mathematics and Statistics, University of Saskatchewan, Saskatoon, Saskatchewan, S7N 5E6, Canada,

Michael Ward; Department of Mathematics, University of British Columbia, Vancouver, British Columbia, V6T 1Z2, Canada (corresponding author)

(Received 15 August 2009)

The method of matched asymptotic expansions is used to calculate a two-term asymptotic expansion for the principal eigenvalue $\lambda(\varepsilon)$ of the Laplacian in a three-dimensional domain Ω with a reflecting boundary that contains N interior traps of asymptotically small radii. In the limit of small trap radii $\varepsilon \rightarrow 0$, this principal eigenvalue is inversely proportional to the average mean first passage time (MFPT), defined as the expected time required for a Brownian particle undergoing free diffusion, and with a uniformly distributed initial starting point in Ω , to be captured by one of the localized traps. The coefficient of the second-order term in the asymptotic expansion of $\lambda(\varepsilon)$ is found to depend on the spatial locations of the traps inside the domain, together with the Neumann Green's function for the Laplacian. For a spherical domain, where this Green's function is known analytically, the discrete variational problem of maximizing the coefficient of the second-order term in the expansion of $\lambda(\varepsilon)$, or correspondingly minimizing the average MFPT, is studied numerically by global optimization methods for $N \leq 20$ traps. Moreover, the effect on the average MFPT of the fragmentation of the trap set is shown to be rather significant for a fixed trap volume fraction when N is not too large. Finally, the method of matched asymptotic expansions is used to calculate the splitting probability in a three-dimensional domain, defined as the probability of reaching a specific target trap from an initial source point before reaching any of the other traps. Some examples of the asymptotic theory for the calculation of splitting probabilities are given for a spherical domain.

Key words: Matched Asymptotic Expansions, Neumann Green's function, Capacitance, Discrete Energy, Global Optimization, Mean First Passage Time, Splitting Probability.

1 Introduction

We consider an optimization problem for the principal eigenvalue of the Laplacian in a bounded three-dimensional domain with a reflecting boundary that is perturbed by the presence of N small traps in the interior of the domain. The perturbed eigenvalue problem is formulated as

$$\Delta u + \lambda u = 0, \quad x \in \Omega \setminus \Omega_a; \quad \int_{\Omega \setminus \Omega_a} u^2 dx = 1, \quad (1.1 a)$$

$$\partial_n u = 0, \quad x \in \partial\Omega, \quad (1.1 b)$$

$$u = 0, \quad x \in \partial\Omega_a \equiv \cup_{j=1}^N \partial\Omega_{\varepsilon_j}. \quad (1.1 c)$$

Here Ω is the unperturbed domain, $\Omega_a \equiv \cup_{j=1}^N \Omega_{\varepsilon_j}$ is a collection of N small interior traps Ω_{ε_j} , for $j = 1, \dots, N$, each of 'radius' $\mathcal{O}(\varepsilon) \ll 1$, and $\partial_n u$ is the outward normal derivative of u on $\partial\Omega$. We assume that $\Omega_{\varepsilon_j} \rightarrow x_j$

uniformly as $\varepsilon \rightarrow 0$, for $j = 1, \dots, N$, and that the traps are well-separated in the sense that $\text{dist}(x_i, x_j) = \mathcal{O}(1)$ for $i \neq j$ and $\text{dist}(x_j, \partial\Omega) = \mathcal{O}(1)$ for $j = 1, \dots, N$.

The primary motivation for considering (1.1) is its relationship to determining the mean first passage time (MFPT) for a Brownian particle wandering inside a three-dimensional domain that contains N localized absorbing traps. Denoting the trajectory of the Brownian particle by $X(t)$, the MFPT $v(x)$ is defined as the expectation value of the time τ taken for the Brownian particle to become absorbed somewhere in $\partial\Omega_a$ starting initially from $X(0) = x \in \Omega$, so that $v(x) = E[\tau | X(0) = x]$. The calculation of $v(x)$ becomes a narrow capture problem in the limit when the volume of the absorbing set $|\partial\Omega_a| = \mathcal{O}(\varepsilon^3)$ is asymptotically small, where $0 < \varepsilon \ll 1$ measures the dimensionless trap radius. Since the MFPT diverges as $\varepsilon \rightarrow 0$, the calculation of the MFPT $v(x)$ constitutes a singular perturbation problem. It is well-known (cf. [11], [25]) that the MFPT $v(x)$ satisfies a Poisson equation with mixed Dirichlet-Neumann boundary conditions, formulated as

$$\Delta v = -\frac{1}{D}, \quad x \in \Omega \setminus \Omega_a, \quad (1.2 a)$$

$$\partial_n v = 0, \quad x \in \partial\Omega; \quad v = 0, \quad x \in \partial\Omega_a = \cup_{j=1}^N \partial\Omega_{\varepsilon_j}, \quad (1.2 b)$$

where D is the diffusivity of the underlying Brownian motion. With respect to a uniform distribution of initial points $x \in \Omega$ for the Brownian walk, the average MFPT, denoted by \bar{v} , is defined by

$$\bar{v} = \chi \equiv \frac{1}{|\Omega|} \int_{\Omega} v(x) dx, \quad (1.3)$$

where $|\Omega|$ is the volume of Ω .

This nature capture problem has wide applications in cellular signal transduction. In particular, in many cases a diffusing molecule must arrive at a localized signaling region within a cell before a signaling cascade can be initiated. Of primary importance then is to determine how quickly such a diffusing molecule can arrive at any one of these localized regions. Our narrow capture problem is closely related to the so-called narrow escape problem, related to the expected time required for a Brownian particle to escape from a confining bounded domain that has N localized windows on an otherwise reflecting boundary. The narrow escape problem has many applications in biophysical modeling (see [2], [11], [27], and the references therein). The narrow escape problem in both two- and three-dimensional confining domains has been studied with a variety of analytical methods in [11], [29], [30], [28], [12], [23], and [3]. In [33], the mean first passage time for a Brownian particle in a 2-D domain with both a boundary and interior trap was calculated asymptotically.

We let $\lambda(\varepsilon)$ denote the first eigenvalue of (1.1), with corresponding eigenfunction $u(x, \varepsilon)$. Clearly, $\lambda(\varepsilon) \rightarrow 0$ as $\varepsilon \rightarrow 0$. For $\varepsilon \rightarrow 0$, a simple calculation shows that $\lambda(\varepsilon)$ is related to the average MFPT χ by $\lambda(\varepsilon) \sim 1/(D\chi)$. One of the main objectives of this paper is to derive a two-term asymptotic expansion for $\lambda(\varepsilon)$ as $\varepsilon \rightarrow 0$. Such a two-term expansion not only provides a more accurate determination, when ε is not too small, of the principal eigenvalue and the corresponding average MFPT, it also provides an explicit formula showing how the locations of the traps within the domain influence these quantities. We emphasize that the leading-order term in the expansion of $\lambda(\varepsilon)$ as $\varepsilon \rightarrow 0$ is independent of the locations of the traps. By examining the coefficient of the second-order term in the expansion of $\lambda(\varepsilon)$ we will formulate a discrete optimization problem for the spatial configuration $\{x_1, \dots, x_N\}$ of

the centers of the N traps of fixed given shapes that maximizes this principal eigenvalue $\lambda(\varepsilon)$, and correspondingly minimizes the average MFPT χ .

Asymptotic expansions for the principal eigenvalue of related eigenvalue problems in perforated multi-dimensional domains, with various boundary conditions on the traps and outer boundary, are given in [31], [20]–[22], [34], [35], [7], [10], [16], and [5] (see also the references therein). In §2 our asymptotic analysis extends the previous results of [20], [21], [35], and [7] for the three-dimensional problem by calculating an extra term in the asymptotic expansion of the principal eigenvalue $\lambda(\varepsilon)$ of (1.1). The resulting two-term asymptotic expansion for $\lambda(\varepsilon)$ given in Principal Result 2.1 of §2 is needed in order to optimize $\lambda(\varepsilon)$ with respect to the spatial configuration $\{x_1, \dots, x_N\}$ of the centers of the traps inside Ω . The coefficient of the second-order term in the asymptotic expansion of $\lambda(\varepsilon)$, which depends on the trap configuration $\{x_1, \dots, x_N\}$, also depends on the Neumann Green's function for the Laplacian and its regular part. This Green's function is given explicitly in Appendix A for the unit sphere. By using this explicit Green's function, in §2.2 global optimization methods are used to obtain numerical results for the trap configurations $\{x_1, \dots, x_N\}$ that maximize the principal eigenvalue $\lambda(\varepsilon)$ of (1.1) for $2 \leq N \leq 20$ identically-shaped traps within the unit sphere.

In §3 we consider the related MFPT problem (1.2). In Principal Result 3.1 we give a two-term asymptotic expansion for the MFPT $v(x)$. For several configurations of traps, we illustrate the effect on $v(x)$ of the spatial distribution of traps inside the unit sphere. By calculating the average MFPT \bar{v} in (1.3) from $\bar{v} \sim 1/(D\lambda)$, we also show the effect on the optimal \bar{v} of the fragmentation of the trap set for a given small trap volume fraction. The fragmentation of the trap set is found to have a significant influence on \bar{v} for a relatively small number of traps.

In §3.2 we consider the related problem of calculating the splitting probability in a three-dimensional domain, defined as the probability of reaching a specific target trap Ω_{ε_1} from the initial source point $x \in \Omega \setminus \Omega_a$, before reaching any of the other surrounding traps Ω_{ε_j} for $j = 2, \dots, N$. The biological applications for the calculation of the splitting probability are discussed in [4], and some of the references therein. For the case of two interior small spherical targets, this problem was considered in Section III (C) of [4] using a pseudo-Green's function technique. Our systematic asymptotic analysis in §3.2 extends this previous analysis of [4] to the case of N targets of possibly different shape. Our analysis highlights the key role of the electrostatic capacitances associated with the targets for the determination of the splitting probability. The theory is illustrated for the case where the confining domain is the unit sphere. The determination of the splitting probability in the context of the two-dimensional narrow escape problem in a circular disk was considered in §5 of [11].

Finally, a few open problems are suggested in §4.

2 Small Traps in a Three-Dimensional Domain

We now use the method of matched asymptotic expansions to derive a two-term expansion for the principal eigenvalue $\lambda(\varepsilon)$ of (1.1) as $\varepsilon \rightarrow 0$. For the problem with no traps, $\lambda_0 = 0$ and $u_0 = |\Omega|^{-1/2}$ is the unperturbed eigenfunction, where $|\Omega|$ denotes the volume of Ω . We expand the principal eigenvalue for (1.1) as

$$\lambda = \varepsilon\lambda_1 + \varepsilon^2\lambda_2 + \dots \quad (2.1)$$

In the outer region away from an $\mathcal{O}(\varepsilon)$ neighborhood of x_j , we expand the outer solution as

$$u = u_0 + \varepsilon u_1 + \varepsilon^2 u_2 + \dots . \quad (2.2)$$

Upon substituting (2.1) and (2.2) into (1.1 a) and (1.1 b), we obtain that u_1 and u_2 satisfy

$$\Delta u_1 = -\lambda_1 u_0, \quad x \in \Omega \setminus \{x_1, \dots, x_N\}; \quad \partial_n u_1 = 0, \quad x \in \partial\Omega; \quad \int_{\Omega} u_1 dx = 0. \quad (2.3)$$

$$\Delta u_2 = -\lambda_2 u_0 - \lambda_1 u_1, \quad x \in \Omega \setminus \{x_1, \dots, x_N\}; \quad \partial_n u_2 = 0, \quad x \in \partial\Omega; \quad \int_{\Omega} u_2 dx = -\frac{|\Omega|^{1/2}}{2} \int_{\Omega} u_1^2 dx. \quad (2.4)$$

The matching of u_1 and u_2 to inner solutions defined in an $\mathcal{O}(\varepsilon)$ neighborhood of each trap will yield singularity conditions for u_1 and u_2 as $x \rightarrow x_j$ for $j = 1, \dots, N$.

In the inner region near the j^{th} trap we introduce the local variables y and $w(y)$ by

$$y = \varepsilon^{-1}(x - x_j), \quad w(y) = u(x_j + \varepsilon y, \varepsilon). \quad (2.5)$$

Upon substituting (2.5) into (1.1 a) and (1.1 c), we obtain that $\Delta_y w = -\varepsilon^2 \lambda w$, where Δ_y denotes the Laplacian in the y variable. We expand the inner solution as

$$w = w_0 + \varepsilon w_1 + \varepsilon^2 w_2 + \dots , \quad (2.6)$$

and then use $\lambda = \mathcal{O}(\varepsilon)$ to obtain the following inner problems for $k = 0, 1, 2$:

$$\Delta_y w_k = 0, \quad y \notin \Omega_j; \quad w_k = 0, \quad y \in \partial\Omega_j. \quad (2.7)$$

Here Ω_j denotes an $\mathcal{O}(\varepsilon^{-1})$ magnification of Ω_{ε_j} so that $\Omega_j = \varepsilon^{-1}\Omega_{\varepsilon_j}$. The appropriate far-field boundary condition for (2.7) is determined by matching w to the outer asymptotic expansion of the eigenfunction.

The matching condition is that the near-field behavior of the outer eigenfunction as $x \rightarrow x_j$ must agree asymptotically with the far-field behavior of the inner eigenfunction as $|y| = \varepsilon^{-1}|x - x_j| \rightarrow \infty$, so that

$$u_0 + \varepsilon u_1 + \varepsilon^2 u_2 + \dots \sim w_0 + \varepsilon w_1 + \varepsilon^2 w_2 + \dots . \quad (2.8)$$

Since $u_0 = |\Omega|^{-1/2}$, the first matching condition is that $w_0 \sim |\Omega|^{-1/2}$ as $|y| \rightarrow \infty$. We then introduce w_c by

$$w_0 = \frac{1}{|\Omega|^{1/2}} (1 - w_c), \quad (2.9)$$

so that from (2.7) with $k = 0$, we get that w_c satisfies

$$\Delta_y w_c = 0, \quad y \notin \Omega_j; \quad w_c = 1, \quad y \in \partial\Omega_j; \quad w_c \rightarrow 0 \quad \text{as} \quad |y| \rightarrow \infty. \quad (2.10 a)$$

This is a classic problem in electrostatics, and it is well-known that the far-field behavior of w_c is (cf. [14])

$$w_c \sim \frac{C_j}{|y|} + \frac{P_j \cdot y}{|y|^3} + \dots \quad \text{as} \quad |y| \rightarrow \infty. \quad (2.10 b)$$

Here C_j is the capacitance of Ω_j and P_j denotes the dipole vector, both determined by the shape of Ω_j . These intrinsic quantities can be found explicitly for different trap shapes such as spheres, ellipsoids, etc..

Upon substituting (2.10 b) into (2.8), we obtain that the matching condition becomes

$$\frac{1}{|\Omega|^{1/2}} + \varepsilon u_1 + \varepsilon^2 u_2 + \cdots \sim \frac{1}{|\Omega|^{1/2}} \left(1 - \frac{\varepsilon C_j}{|x - x_j|} - \frac{\varepsilon^2 P_j \cdot (x - x_j)}{|x - x_j|^3} \right) + \varepsilon w_1 + \varepsilon^2 w_2 + \cdots. \quad (2.11)$$

Therefore, we require that u_1 has the singular behavior $u_1 \sim -|\Omega|^{-1/2} C_j / |x - x_j|$ as $x \rightarrow x_j$ for $j = 1, \dots, N$. The problem (2.3) for u_1 with this singularity behavior can be written in Ω in terms of the Dirac distribution as

$$\Delta u_1 = -\lambda_1 u_0 + \frac{4\pi}{|\Omega|^{1/2}} \sum_{j=1}^N C_j \delta(x - x_j), \quad x \in \Omega; \quad \partial_n u_1 = 0, \quad x \in \partial\Omega, \quad (2.12)$$

with $\int_{\Omega} u_1 dx = 0$. Upon using the divergence theorem, and recalling that $u_0 = |\Omega|^{-1/2}$, we determine λ_1 as

$$\lambda_1 = \frac{4\pi}{|\Omega|} \sum_{j=1}^N C_j. \quad (2.13)$$

This leading order asymptotics is Ozawa's result [20], and since it does not depend on the trap locations it does not indicate how to optimize λ . As such, we must extend the calculation to one higher order.

To solve (2.12), we introduce the Neumann Green's function $G(x; \xi)$, which satisfies

$$\Delta G = \frac{1}{|\Omega|} - \delta(x - \xi), \quad x \in \Omega; \quad \partial_n G = 0, \quad x \in \partial\Omega, \quad (2.14 a)$$

$$G(x; \xi) = \frac{1}{4\pi|x - \xi|} + R(x; \xi); \quad \int_{\Omega} G(x; \xi) dx = 0. \quad (2.14 b)$$

Here $R(x; \xi)$ is called the regular part of $G(x; \xi)$, and $R(\xi; \xi)$ is referred to as the self-interaction term. In terms of G , the unique solution to (2.12), which satisfies $\int_{\Omega} u_1 dx = 0$, is simply

$$u_1 = -\frac{4\pi}{|\Omega|^{1/2}} \sum_{k=1}^N C_k G(x; x_k). \quad (2.15)$$

Next, we expand u_1 in (2.15) as $x \rightarrow x_j$. Upon using (2.14 b) to obtain the local behavior of G , we obtain

$$u_1 \sim -\frac{C_j}{|\Omega|^{1/2}|x - x_j|} + A_j \quad \text{as } x \rightarrow x_j; \quad A_j = -\frac{4\pi}{|\Omega|^{1/2}} \left(C_j R_{j,j} + \sum_{\substack{k=1 \\ k \neq j}}^N C_k G_{j,k} \right). \quad (2.16)$$

Here we have defined $R_{j,j} \equiv R(x_j; x_j)$ and $G_{j,k} \equiv G(x_j; x_k)$. Upon substituting this expression into the matching condition (2.11), we obtain

$$\frac{1}{|\Omega|^{1/2}} + \varepsilon \left(-\frac{C_j}{|\Omega|^{1/2}|x - x_j|} + A_j \right) + \varepsilon^2 u_2 + \cdots \sim \frac{1}{|\Omega|^{1/2}} \left(1 - \frac{\varepsilon C_j}{|x - x_j|} - \frac{\varepsilon^2 P_j \cdot (x - x_j)}{|x - x_j|^3} \right) + \varepsilon w_1 + \varepsilon^2 w_2 + \cdots. \quad (2.17)$$

We then conclude that $w_1 \sim A_j$ as $|y| \rightarrow \infty$. The solution w_1 to (2.7) is

$$w_1 = A_j (1 - w_c) \sim A_j \left(1 - \frac{C_j}{|y|} + \cdots \right) \quad \text{as } |y| \rightarrow \infty, \quad (2.18)$$

where w_c is the solution to (2.10). Next, we write the far-field behavior in (2.18) in outer variables and substitute the resulting expression into the right-hand side of the matching condition (2.17) to identify the terms of $\mathcal{O}(\varepsilon^2)$. In

this way, we obtain that the outer eigenfunction u_2 must have the following singularity behavior as $x \rightarrow x_j$:

$$u_2 \sim -\frac{A_j C_j}{|x - x_j|} - \frac{P_j \cdot (x - x_j)}{|x - x_j|^3} \quad \text{as } x \rightarrow x_j, \quad j = 1, \dots, N. \quad (2.19)$$

The problem (2.4) for u_2 , together with singularity behavior (2.19), can be written in Ω in terms of the Dirac distribution as

$$\Delta u_2 = -\lambda_2 u_0 - \lambda_1 u_1 + 4\pi \sum_{j=1}^N A_j C_j \delta(x - x_j) - 4\pi \sum_{j=1}^N P_j \cdot \nabla \delta(x - x_j), \quad x \in \Omega, \quad (2.20)$$

with $\partial_n u_2 = 0$ for $x \in \partial\Omega$. Then, applying the divergence theorem to (2.20), and using $\int_{\Omega} u_1 dx = 0$, we get

$$\lambda_2 = \frac{4\pi}{|\Omega|^{1/2}} \sum_{j=1}^N A_j C_j. \quad (2.21)$$

We remark that this eigenvalue correction λ_2 does not depend on the dipole vector P_j defined in (2.10 b).

Next, it is convenient to introduce the capacitance vector \mathbf{c} and the symmetric Neumann Green's matrix \mathcal{G} by

$$\mathcal{G} \equiv \begin{pmatrix} R_{1,1} & G_{1,2} & \cdots & G_{1,N} \\ G_{2,1} & \ddots & \ddots & \vdots \\ \vdots & \ddots & \ddots & G_{N-1,N} \\ G_{N,1} & \cdots & G_{N,N-1} & R_{N,N} \end{pmatrix}, \quad \mathbf{c} \equiv \begin{pmatrix} C_1 \\ \vdots \\ C_N \end{pmatrix}. \quad (2.22)$$

Here C_j is the capacitance defined in (2.10 b), and $G_{i,j} \equiv G(x_i; x_j)$ for $i \neq j$ is the Neumann Green's function of (2.14) with self-interaction $R_{j,j} \equiv R(x_j; x_j)$. Upon substituting (2.13) and (2.21) into (2.1), we obtain the following main result:

Principal Result 2.1: *In the limit of small trap radius, $\varepsilon \rightarrow 0$, the principal eigenvalue $\lambda(\varepsilon)$ of (1.1) has the two-term asymptotic expansion*

$$\lambda(\varepsilon) \sim \frac{4\pi\varepsilon N}{|\Omega|} \bar{C} - \frac{16\pi^2\varepsilon^2}{|\Omega|} p_c(x_1, \dots, x_N). \quad (2.23 a)$$

Here $\bar{C} \equiv N^{-1}(C_1 + \dots + C_N)$ and $p_c(x_1, \dots, x_N)$ is the discrete sum defined in terms of the entries $\mathcal{G}_{i,j}$ of the Green's matrix \mathcal{G} of (2.22) by

$$p_c(x_1, \dots, x_N) \equiv \mathbf{c}^T \mathcal{G} \mathbf{c} = \sum_{i=1}^N \sum_{j=1}^N C_i C_j \mathcal{G}_{i,j}. \quad (2.23 b)$$

The corresponding eigenfunction u is given asymptotically in the outer region $|x - x_j| \gg \mathcal{O}(\varepsilon)$ for $j = 1, \dots, N$ by

$$u \sim \frac{1}{|\Omega|^{1/2}} - \frac{4\pi\varepsilon}{|\Omega|^{1/2}} \sum_{j=1}^N C_j G(x; x_j) + \mathcal{O}(\varepsilon^2). \quad (2.23 c)$$

For $\varepsilon \ll 1$, the principal eigenvalue $\lambda(\varepsilon)$ is maximized when the trap configuration $\{x_1, \dots, x_N\}$ is chosen to minimize $p_c(x_1, \dots, x_N)$. For N identical traps with a common capacitance C , (2.23 a) reduces to

$$\lambda(\varepsilon) \sim \frac{4\pi\varepsilon N C}{|\Omega|} \left[1 - \frac{4\pi\varepsilon C}{N} p(x_1, \dots, x_N) \right], \quad p(x_1, \dots, x_N) \equiv \mathbf{e}^T \mathcal{G} \mathbf{e} = \sum_{i=1}^N \sum_{j=1}^N \mathcal{G}_{i,j}. \quad (2.23 d)$$

Trap Shape $\Omega_j = \varepsilon^{-1}\Omega_{\varepsilon_j}$	Capacitance C_j
sphere of radius a	$C_j = a$
hemisphere of radius a	$C_j = 2a \left(1 - \frac{1}{\sqrt{3}}\right)$
flat disk of radius a	$C_j = \frac{2a}{\pi}$
prolate spheroid with semi-major and minor axes a, b	$C_j = \frac{\sqrt{a^2 - b^2}}{\cosh^{-1}(a/b)}$
oblate spheroid with semi-major and minor axes a, b	$C_j = \frac{\sqrt{a^2 - b^2}}{\cos^{-1}(b/a)}$
ellipsoid with axes $a, b,$ and c	$C_j = 2 \left(\int_0^\infty (a^2 + \eta)^{-1/2} (b^2 + \eta)^{-1/2} (c^2 + \eta)^{-1/2} d\eta \right)^{-1}$

 Table 1. Capacitance C_j of some simple trap shapes, defined from the solution to (2.10).

The capacitance C_j , defined in (2.10), has two key properties. Firstly, it is invariant under rotations of the trap shape. Secondly, with respect to all trap shapes Ω_j in (2.10) of the same volume, C_j is minimized for a spherical-shaped trap (cf. [32]). Although C_j must in general be calculated numerically from (2.10) when Ω_j has an arbitrary shape, it is known analytically for some simple shapes, as summarized in Table 1. The capacitance C_j is also known in a few other situations. For instance, for the case of two overlapping identical spheres of radius εa_j that intersect at exterior angle ψ , with $0 < \psi < \pi$, then C_j is given by (cf. [6])

$$C_j = 2 a_j \sin\left(\frac{\psi}{2}\right) \int_0^\infty \left[1 - \tanh(\pi\tau) \tanh\left(\frac{\psi\tau}{2}\right)\right] d\tau. \quad (2.24)$$

For $\psi \rightarrow 0$, (2.24) reduces to the well-known result $C_j = 2a_j \log 2$ for the capacitance of two touching spheres.

Principal Result 2.1 also holds when there is a cluster of traps localized within an $\mathcal{O}(\varepsilon)$ region near some location $x_j \in \Omega$. For this case, C_j is still determined from (2.10), provided that we replace Ω_j by a multi-connected set of the form $\Omega_j = \bigcup_{k=1}^{k_j} \Omega_{jk}$, where k_j denotes the number of distinct traps in the j^{th} clustering region. This capacitance is known analytically for the special case of two identical spheres of radius εa_j clustered near $x = x_j$, where εd_j is the distance between the centers of the two spheres, with $d_j > 2a_j$. For this case, C_j is given by (cf. [36], [17])

$$C_j = 2a_j \sinh(\beta) \sum_{n=1}^{\infty} \frac{1}{\sinh(n\beta)}, \quad \cosh(\beta) = \frac{d_j}{2a_j}. \quad (2.25)$$

2.1 Numerical Results for the Unit Sphere

We now optimize the coefficient of the second-order term in the asymptotic expansion of λ in (2.23 d) of Principal Result 2.1 for the special case when Ω is a sphere of radius one that contains N small identically-shaped traps of a common “radius” ε . By using a simple scaling argument, our results below for this special case of a unit sphere also apply to the more general case of a sphere of radius L that contains N small identical traps of a common “radius” σ . By scaling lengths by L , Principal Result 2.1 holds provided that we multiply λ in this result by L^{-2} and identify ε as $\varepsilon = \sigma/L \ll 1$. Therefore, we need only consider the case of the unit sphere.

As shown in Appendix A, the Neumann Green's function of (2.14) for the unit sphere is given explicitly by

$$G(x; \xi) = \frac{1}{4\pi|x - \xi|} + \frac{1}{4\pi|x||x' - \xi|} + \frac{1}{4\pi} \log \left(\frac{2}{1 - |x||\xi| \cos \theta + |x||x' - \xi|} \right) + \frac{1}{6|\Omega|} (|x|^2 + |\xi|^2) - \frac{7}{10\pi}, \quad (2.26 a)$$

where $|\Omega| = 4\pi/3$. Here $x' = x/|x|^2$ is the image point to x outside the unit sphere, and θ is the angle between ξ and x , i.e. $\cos \theta = x \cdot \xi / |x||\xi|$, where \cdot denotes the dot product. This result, without the constant term on the right-hand side of (2.26 a), is given in [15] without derivation.

To calculate $R(\xi; \xi)$ from (2.26 a) we take the limit of $G(x, \xi)$ as $x \rightarrow \xi$ and extract the nonsingular part of the resulting expression. Setting $x = \xi$ and $\theta = 0$ in (2.26 a), we obtain $|x' - \xi| = -|\xi| + 1/|\xi|$, so that

$$R(\xi, \xi) = \frac{1}{4\pi(1 - |\xi|^2)} + \frac{1}{4\pi} \log \left(\frac{1}{1 - |\xi|^2} \right) + \frac{|\xi|^2}{4\pi} - \frac{7}{10\pi}. \quad (2.26 b)$$

Consider the special case of two concentric spheres of radius $r = 1$ and $r = \varepsilon$. For this case, the principal eigenvalue and corresponding radially symmetric (unnormalized) eigenfunction satisfy

$$u = \frac{1}{r} \left[\sin(\sqrt{\lambda}r) - \tan(\sqrt{\lambda}\varepsilon) \cos(\sqrt{\lambda}r) \right], \quad \tan(\sqrt{\lambda}) = \frac{\sqrt{\lambda} + \tan(\sqrt{\lambda}\varepsilon)}{1 - \sqrt{\lambda} \tan(\sqrt{\lambda}\varepsilon)}. \quad (2.27)$$

For $\varepsilon \rightarrow 0$, the principal root to the transcendental equation (2.27) is readily calculated as $\lambda \sim 3\varepsilon + 27\varepsilon^2/5$. This result for λ agrees with that given in (2.23 a) of Principal Result 2.1, as seen upon substituting $C_1 = 1$ (see Table 1) and $R_{1,1} = R(0; 0) = -9/(20\pi)$, from (2.26 b), into (2.23 a).

Next, we compute optimal spatial arrangements $\{x_1, \dots, x_N\}$ of $N \geq 2$ identically shaped traps inside the unit sphere that minimizes $p(x_1, \dots, x_N)$ in (2.23 d), or equivalently maximizes the coefficient of the second-order term in ε in the asymptotic expansion of $\lambda(\varepsilon)$ given in (2.23 d). To simplify the computation, we will minimize the function $\mathcal{H}_{\text{ball}}$ defined in terms of p of (2.23 d) by

$$\mathcal{H}_{\text{ball}} \equiv \sum_{i=1}^N \sum_{j=1}^N \tilde{\mathcal{G}}_{i,j} = \sum_{i=1}^N \sum_{j=1}^N \left((1 - \delta_{ij}) \tilde{\mathcal{G}}_{ij} + \delta_{ij} \tilde{\mathcal{R}}_{ii} \right), \quad p(x_1, \dots, x_N) = \frac{\mathcal{H}_{\text{ball}}}{4\pi} - \frac{7N^2}{10\pi}, \quad (2.28)$$

where $\delta_{ij} = 0$ if $i \neq j$ and $\delta_{jj} = 1$. Here we have defined $\tilde{\mathcal{G}}_{i,j}$, $\tilde{\mathcal{G}}_{i,i}$ and $\tilde{\mathcal{R}}_{j,j}$ by $\tilde{\mathcal{G}}_{i,j} = 4\pi(\mathcal{G}_{i,j} - B)$, $\tilde{\mathcal{G}}_{i,i} \equiv 4\pi(\mathcal{G}_{i,i} - B)$, and $\tilde{\mathcal{R}}_{j,j} \equiv 4\pi(\mathcal{R}_{j,j} - B)$, where $B = -7/(10\pi)$ and $\mathcal{G}_{i,j}$ and $\mathcal{R}_{j,j}$ are obtained from (2.26).

Various numerical methods for global optimization are available (cf. [24], [13], [26]), including methods for non-smooth optimization and optimization with constraints. For low-dimensional problems, exact methods are available, whereas for higher-dimensional problems one often must use heuristic strategies, including evolution algorithms and simulated annealing. The following methods were used to confirm our numerical optimization results for (2.28):

- (1) *The Extended Cutting Angle method (ECAM)*. This deterministic global optimization technique is applicable to Lipschitz functions. Within the algorithm, a sequence of piecewise linear lower approximations to the objective function is constructed. The sequence of the corresponding solutions to these relaxed problems converges to the global minimum of the objective function (cf. [1]).

N	$\mathcal{H}_{\text{ball}}^{(a)}$	Spherical radii $r_1 = \dots = r_N$	$\mathcal{H}_{\text{ball}}^{(b)}$	Spherical radii $r_2 = \dots = r_N$ ($r_1 = 0$)
2	7.2763	0.429	9.0316	0.563
3	18.5047	0.516	20.3664	0.601
4	34.5635	0.564	36.8817	0.626
5	56.2187	0.595	58.1823	0.645
6	82.6490	0.618	85.0825	0.659
7	115.016	0.639	116.718	0.671
8	152.349	0.648	154.311	0.680
9	195.131	0.659	196.843	0.688
10	243.373	0.668	244.824	0.694
11	297.282	0.676	297.283	0.700
12	355.920	0.683	357.371	0.705
13	420.950	0.689	421.186	0.710
14	491.011	0.694	491.415	0.713
15	566.649	0.698	566.664	0.717
16	647.738	0.702	647.489	0.720
17	734.344	0.706	733.765	0.722
18	826.459	0.709	825.556	0.725
19	924.360	0.712	922.855	0.727
20	1027.379	0.715	1025.94	0.729

Table 2. Numerically computed minimal values of the discrete energy functions $\mathcal{H}_{\text{ball}}^{(a)}$ and $\mathcal{H}_{\text{ball}}^{(b)}$ for the optimal arrangement of N -traps within a unit sphere, as computed using the DSO method. The numerically computed minimum value of $\mathcal{H}_{\text{ball}}$ in (2.28) is shown in bold face.

(2) *Dynamical Systems Based Optimization (DSO)*. A dynamical system is constructed, using a number of sampled values of the objective function to introduce “forces”. The evolution of such a system yields a descent trajectory converging to lower values of the objective function. The algorithm continues sampling the domain until it converges to a stationary point (cf. [18]).

Our computational results given below for the minimization of (2.28) were obtained by using the open software library GANSO (cf. [8]), where both the ECAM and DSO methods are implemented.

Inside the unit sphere, the location x_j of every trap is written in spherical coordinates (r_j, θ_j, ϕ_j) , where r_j is the spherical radius, θ_j is the latitude, and ϕ_j is the longitude. For the first trap location, x_1 , we take $\theta_1 = \phi_1 = 0$, while for the second trap we take $\phi_2 = 0$. These constraints eliminate the effect of the rotational symmetry of the sphere. Then, for the case of N traps in the unit sphere, one has a global optimization problem involving the $3N - 3$ parameters $0 \leq r_j \leq 1$ for $j = 2, \dots, N$, $0 < \theta_j \leq \pi$ for $j = 2, \dots, N$, and $0 \leq \phi_j < 2\pi$ for $j = 3, \dots, N$.

As an “initial guess” for the global optimization numerical routines, we let all traps have spherical radius $r_j = 1/2$, and we place the traps x_2, \dots, x_N equally spaced on the equator $\theta_j = \pi/2$, where $\phi_j = 2\pi(j - 2)/(N - 1)$

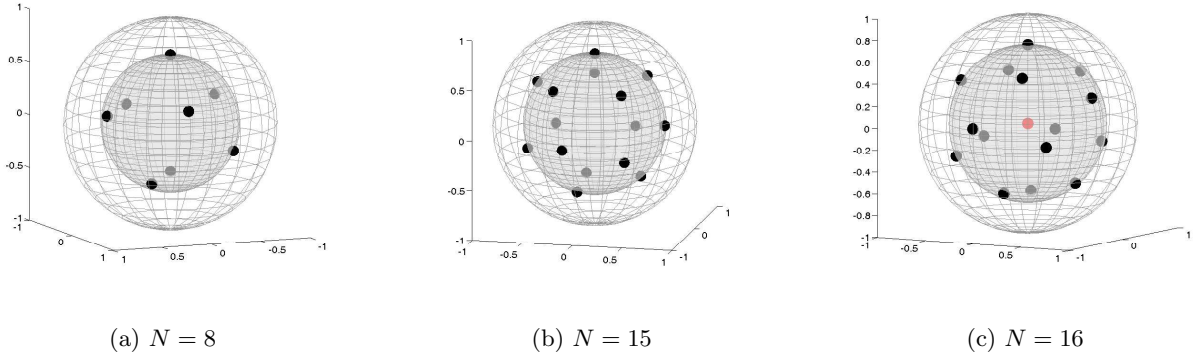


FIGURE 1. Numerically computed optimal spatial arrangements of traps inside a unit sphere. For $N = 8$ and $N = 15$ all traps are on an interior sphere. For $N = 16$ there is one trap at the origin, while 15 traps are on an interior sphere.

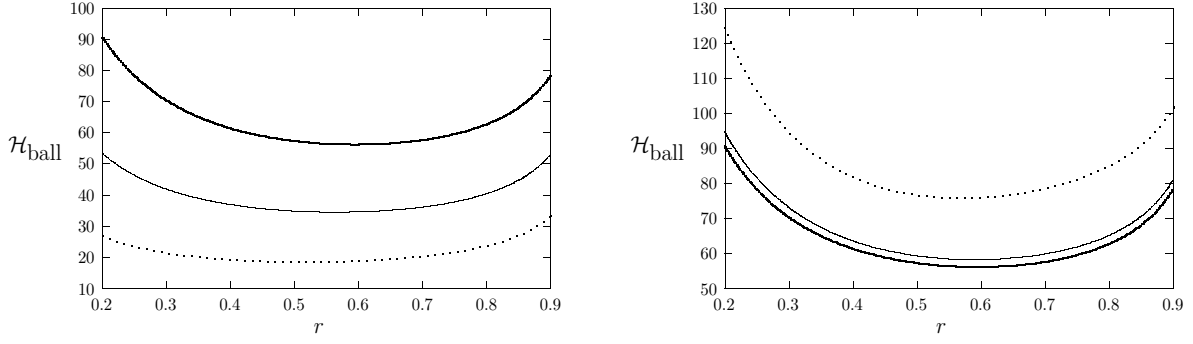
for $j = 2, \dots, N$. By using the DSO and ECAM methods, as outlined above, we numerically compute optimal arrangements of the locations $N = 2, \dots, 20$ spherical traps inside the unit sphere that minimizes $\mathcal{H}_{\text{ball}}$ in (2.28).

The optimal trap pattern when N is small, consisting of N traps on one inner sphere, is found to switch to an optimal pattern with $N - 1$ traps on an inner sphere and one at the origin as N is increased. We compare the minimal values of the discrete energy $\mathcal{H}_{\text{ball}}$ in (2.28) for the case (a) when all traps are forced to lie on one sphere ($\mathcal{H}_{\text{ball}}^{(a)}$), and in the case (b) when one trap remains at the origin ($r_1 = 0$), while the remaining traps lie on one inner sphere ($\mathcal{H}_{\text{ball}}^{(b)}$). These optimal energy values and the corresponding inner sphere radii, computed with the DSO method, are given in Table 2. For each N with $2 \leq N \leq 15$, our results show that the optimal configuration has N traps located *on a single inner sphere* within the unit sphere. The case $N = 16$ is the smallest value of N that deviates from this rule. In particular, for $16 \leq N \leq 20$, there is one trap located at the origin ($r_1 = 0$), while the remaining $N - 1$ traps are located on one interior sphere so that $r_2 = \dots = r_N$.

We remark that the numerically computed minima of the energy function $\mathcal{H}_{\text{ball}}$ in (2.28) were computed directly using the ECAM and DSO methods, and the results obtained were found to coincide with the results shown in Table 2 computed from the restricted optimization problem associated with $\mathcal{H}_{\text{ball}}^{(a)}$ for $2 \leq N \leq 15$ and with $\mathcal{H}_{\text{ball}}^{(b)}$ for $N = 16, 17, 18$. In Fig. 1 we show the numerically computed optimal spatial arrangements of traps for $N = 8, 15, 16$.

Next, we illustrate the sensitivity of the discrete energy $\mathcal{H}_{\text{ball}}$ of (2.28) for non-optimally located traps in the unit sphere. In Fig. 2(a) we plot $\mathcal{H}_{\text{ball}}$ versus the radius r of an inner sphere, when either $N = 3$, $N = 4$, or $N = 5$ traps are optimally placed on the surface of this inner sphere. The minimum value for each of the curves in Fig. 2(a) with respect to r is the optimal result given in Table 2. In Fig. 2(b) we plot $\mathcal{H}_{\text{ball}}$ versus the inner sphere radius r for three different arrangements of $N = 5$ traps on the surface of the inner sphere (see the caption of Fig. 2(b)).

The numerical optimization problem becomes increasingly difficult to solve as N increases, due to the occurrence of many local minima. An open problem is to reliably compute the global minimum of the discrete energy $\mathcal{H}_{\text{ball}}$ for N large and to determine a scaling law for it valid as $N \rightarrow \infty$.


 (a) $\mathcal{H}_{\text{ball}}$ vs. r for $N = 3, 4, 5$

 (b) $\mathcal{H}_{\text{ball}}$ vs. r for $N = 5$

FIGURE 2. Left figure: the discrete energy $\mathcal{H}_{\text{ball}}$ of (2.28) for $N = 3$ (dashed curve), $N = 4$ (solid curve), and $N = 5$ (heavy solid curve) optimally placed traps on the surface of an inner sphere of radius r . The minimum value for each of these curves is the optimal result of Table 2. Right figure: $\mathcal{H}_{\text{ball}}$ versus r for three different arrangements of $N = 5$ traps on an inner sphere of radius r : optimally spaced traps (heavy solid curve); five traps on the equatorial plane (solid curve); five traps on the azimuthal plane $\theta = \pi/4$ (dashed curve).

3 Mean First Passage Time and Splitting Probabilities

The mean first passage time (MFPT) $v(x)$ is the expectation value of the time τ taken for a Brownian particle starting from x to become absorbed somewhere in the multiply-connected trap boundary set $\partial\Omega_a \equiv \bigcup_{j=1}^N \partial\Omega_{\varepsilon_j}$. It is well-known (cf. [11], [25]) that the MFPT $v(x)$ satisfies

$$\Delta v = -\frac{1}{D}, \quad x \in \Omega \setminus \Omega_a \equiv \bigcup_{j=1}^N \Omega_{\varepsilon_j}; \quad v = 0, \quad x \in \partial\Omega_a; \quad \partial_n v = 0, \quad x \in \partial\Omega, \quad (3.1)$$

where D is the constant diffusivity for the underlying Brownian motion. We assume that $\Omega_{\varepsilon_j} \rightarrow x_j$ uniformly as $\varepsilon \rightarrow 0$, for $j = 1, \dots, N$, and that the traps are well-separated.

The mean first passage time v is readily calculated by using the matched asymptotic approach of §2.1. Alternatively, v can be calculated by representing it as an eigenfunction expansion in terms of the normalized eigenfunctions ϕ_k and eigenvalues λ_k for $k \geq 1$ of (1.1). In the trap-free domain $\Omega_p = \Omega \setminus \Omega_a$, we readily derive that

$$v = \frac{1}{D} \left[\frac{\phi_1}{\lambda_1} \left(\int_{\Omega_p} \phi_1 dx \right) + \sum_{k=2}^{\infty} \frac{\phi_k}{\lambda_k} \left(\int_{\Omega_p} \phi_k dx \right) \right]. \quad (3.2)$$

For $\varepsilon \rightarrow 0$, the principal eigenpair λ_1, ϕ_1 , are given in (2.23 a) and (2.23 c), respectively. They satisfy $\int_{\Omega_p} \phi_1 dx = 1 + \mathcal{O}(\varepsilon^2)$ and $\lambda_1 = \mathcal{O}(\varepsilon)$. Next, we give a rough estimate of the asymptotic order of the infinite sum in (3.2). This infinite sum does converge for each fixed ε , since $\lambda_k = \mathcal{O}(k^2)$ as $k \rightarrow \infty$. However, for each fixed k with $k > 2$, we have that $\lambda_k = \lambda_{k0} + \mathcal{O}(\varepsilon)$ as $\varepsilon \rightarrow 0$, where $\lambda_{k0} > 0$ for $k \geq 2$ are the eigenvalues of the Laplacian in the trap-free unit sphere with homogeneous Neumann boundary condition. In addition, for each fixed k with $k \geq 2$, we have that $\int_{\Omega_p} \phi_k dx = \mathcal{O}(\varepsilon)$, due to the near orthogonality of ϕ_k and 1 as $\varepsilon \rightarrow 0$ when $k \geq 2$. In this way, for $\varepsilon \rightarrow 0$, the

infinite sum in (3.2) contributes at most an $\mathcal{O}(\varepsilon)$ term, and consequently it can be neglected in comparison with the leading term in (3.2). This leads to the following result:

Principal Result 3.1: *In the limit $\varepsilon \rightarrow 0$ of small trap radius, the mean first passage time v , satisfying (3.1), is given asymptotically in the outer region $|x - x_j| \gg \mathcal{O}(\varepsilon)$ for $j = 1, \dots, N$ by*

$$v \sim \frac{|\Omega|}{4\pi N \bar{C} D \varepsilon} \left[1 - 4\pi\varepsilon \sum_{j=1}^N C_j G(x; x_j) + \frac{4\pi\varepsilon}{N\bar{c}} p_c(x_1, \dots, x_N) + \mathcal{O}(\varepsilon^2) \right]. \quad (3.3 a)$$

Here $\bar{C} = N^{-1}(C_1 + \dots + C_N)$, and $p_c(x_1, \dots, x_N)$ is the weighted discrete sum in (2.23 b). The average mean first passage time $\bar{v} \sim |\Omega|^{-1} \int_{\Omega} v dx$, based on a uniform distribution of starting points x , satisfies

$$\bar{v} \sim \frac{1}{D|\Omega|\lambda_1} + \mathcal{O}(\varepsilon) = \frac{|\Omega|}{4\pi N \bar{C} D \varepsilon} \left[1 + \frac{4\pi\varepsilon}{N\bar{C}} p_c(x_1, \dots, x_N) + \mathcal{O}(\varepsilon^2) \right]. \quad (3.3 b)$$

For the special case of N traps with a common capacitance $C = C_j$ for $j = 1, \dots, N$ inside the unit sphere, then \bar{v} in (3.3 b) becomes

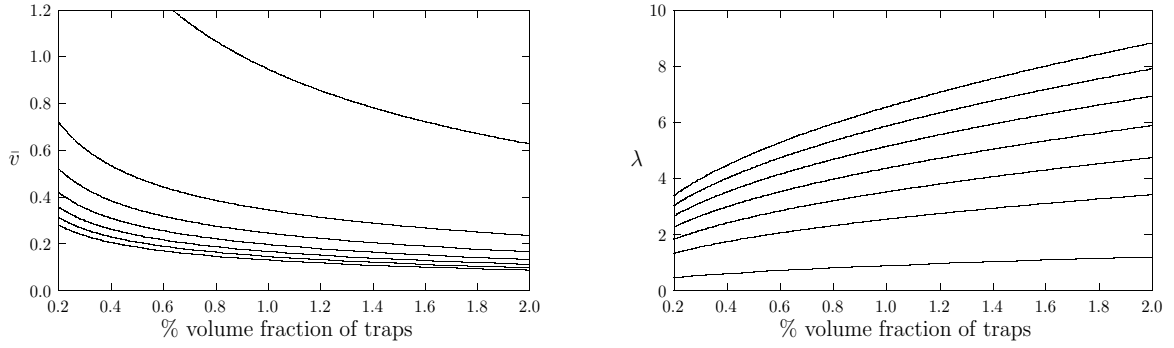
$$\bar{v} \sim \frac{|\Omega|}{D} \left[\frac{1}{4\pi\varepsilon N C} + \frac{1}{N^2} p(x_1, \dots, x_N) \right], \quad p(x_1, \dots, x_N) = \sum_{i=1}^N \sum_{j=1}^N \mathcal{G}_{ij} = \frac{\mathcal{H}_{\text{ball}}}{4\pi} - \frac{7N^2}{10\pi}, \quad (3.4)$$

where $\mathcal{H}_{\text{ball}}$ is the discrete energy defined in (2.28). Next, we use (3.4) to illustrate the effect on \bar{v} of trap clustering. For $N = 20$ optimally placed spherical traps of a common radius ε , we set $C = 1$ and use the last entry for $\mathcal{H}_{\text{ball}}$ in Table 2 for $N = 20$ to evaluate p in (3.4). In contrast, suppose that there are $N = 10$ clusters of two touching spheres of a common radius ε inside the unit sphere. Assume that the clusters are optimally located within the unit sphere. For this arrangement, we set $N = 10$ in (3.4), and use the capacitance $C = 2 \log 2$ of two touching spheres, together with optimal value for $\mathcal{H}_{\text{ball}}$ given in Table 2 for $N = 10$. In this way, we obtain

$$\bar{v} \sim \frac{|\Omega|}{D} \left(\frac{1}{80\pi\varepsilon} - 0.01871 \right), \quad (\text{no trap clustering}); \quad \bar{v} \sim \frac{|\Omega|}{D} \left(\frac{1}{80\pi\varepsilon \log 2} - 0.02915 \right), \quad (\text{trap clustering}). \quad (3.5)$$

Therefore, to leading order, this case of trap clustering increases the average MFPT by a factor of $1/\log 2$.

Principal Result 3.1 can be used to show the influence of the number N of distinct subregions comprising the trap set. We consider N spherical traps of a common radius ε inside the unit sphere. We denote the percentage trap volume fraction by $100f$, where $f = 4\pi\varepsilon^3 N / (3|\Omega|) = \varepsilon^3 N$. In Fig. 3(a) we plot \bar{v} , given in (3.4) with $C = 1$, versus the trap volume percentage fraction $100f$ corresponding to the optimal arrangement of $N = 5, 8, 11, 14, 17, 20$ traps, as computed from the global optimization routine in §2.2 (see Table 2). In this figure we also plot \bar{v} for a single large trap with the same trap volume fraction. We conclude that even when f is small, the effect of fragmentation of the trap set is rather significant. In Fig. 3(b) we plot the corresponding principal eigenvalue λ of (2.23 d) versus the percentage trap volume fraction.


 (a) \bar{v} versus $100f$

 (b) λ versus $100f$

FIGURE 3. The average MFPT \bar{v} in (3.3 b) with $D = 1$ and the principal eigenvalue λ of (2.23 d) versus the percentage trap volume fraction $100f = 100\varepsilon^3 N$ for the optimal arrangement of N identical traps of a common radius ε in the unit sphere. Left figure: \bar{v} versus $100f$ for $N = 1, 5, 8, 11, 14, 17, 20$ (top to bottom curves). Right figure: λ versus $100f$ for $N = 1, 5, 8, 11, 14, 17, 20$ (bottom to top curves).

3.1 Splitting Probabilities

Next, we use the method of matched asymptotic expansions to calculate the splitting probabilities of [4]. The splitting probability $u(x)$ is defined as the probability of reaching a specific target trap Ω_{ε_1} from the initial source point $x \in \Omega \setminus \Omega_a$, before reaching any of the other surrounding traps Ω_{ε_j} for $j = 2, \dots, N$. Then, it is well-known that u satisfies (cf. [4])

$$\Delta u = 0, \quad x \in \Omega \setminus \Omega_a \equiv \cup_{j=1}^N \Omega_{\varepsilon_j}; \quad \partial_n u = 0, \quad x \in \partial\Omega, \quad (3.6 a)$$

$$u = 1, \quad x \in \partial\Omega_{\varepsilon_1}; \quad u = 0, \quad x \in \cup_{j=2}^N \partial\Omega_{\varepsilon_j}. \quad (3.6 b)$$

In the outer region, we expand u as

$$u = u_0 + \varepsilon u_1 + \varepsilon^2 u_2 + \dots. \quad (3.7)$$

Here u_0 is an unknown constant, and u_k for $k = 1, 2$ satisfies

$$\Delta u_k = 0, \quad x \in \Omega \setminus \{x_1, \dots, x_N\}; \quad \partial_n u_k = 0, \quad x \in \partial\Omega, \quad (3.8)$$

with certain singularity conditions as $x \rightarrow x_j$ for $j = 1, \dots, N$ determined upon matching to the inner solution.

In the inner region near the j^{th} trap, we expand the inner solution $w(y) \equiv u(x_j + \varepsilon y)$, with $y \equiv \varepsilon^{-1}(x - x_j)$, as

$$w = w_0 + \varepsilon w_1 + \dots. \quad (3.9)$$

Upon substituting (3.9) into (3.6 a) and (3.6 b), we obtain that w_0 and w_1 satisfy

$$\Delta_y w_0 = 0, \quad y \notin \Omega_j; \quad w_0 = \delta_{j1}, \quad y \in \partial\Omega_j, \quad (3.10 a)$$

$$\Delta_y w_1 = 0, \quad y \notin \Omega_j; \quad w_1 = 0, \quad y \in \partial\Omega_j. \quad (3.10 b)$$

Here $\Omega_j = \varepsilon^{-1}\Omega_{\varepsilon_j}$, and δ_{j1} is Kronecker's symbol. The far-field boundary conditions for w_0 and w_1 are determined by the matching condition as $x \rightarrow x_j$ between the the inner and outer expansions (3.9) and (3.7), respectively, written as

$$u_0 + \varepsilon u_1 + \varepsilon^2 u_2 + \dots \sim w_0 + \varepsilon w_1 + \dots. \quad (3.11)$$

The first matching condition is that $w_0 \sim u_0$ as $|y| \rightarrow \infty$, where u_0 is an unknown constant. Then, the solution for w_0 in the j^{th} inner region is given by

$$w_0 = u_0 + (\delta_{j1} - u_0) w_c(y), \quad (3.12)$$

where w_c is the solution to (2.10 a). Upon, using the far-field asymptotic behavior (2.10 b) for w_c , we obtain that

$$w_0 \sim u_0 + (\delta_{j1} - u_0) \left(\frac{C_j}{|y|} + \frac{P_j \cdot y}{|y|^3} \right), \quad \text{as } y \rightarrow \infty. \quad (3.13)$$

Here C_j and P_j are the capacitance and dipole vector of Ω_j , respectively, as defined in (2.10 b).

From (3.13) and (3.11), we conclude that u_1 satisfies (3.8) with singular behavior $u_1 \sim (\delta_{j1} - u_0) C_j / |x - x_j|$ as $x \rightarrow x_j$ for $j = 1, \dots, N$. Therefore, in terms of the Dirac distribution, u_1 satisfies

$$\Delta u_1 = -4\pi \sum_{j=1}^N (\delta_{j1} - u_0) C_j \delta(x - x_j), \quad x \in \Omega; \quad \partial_n u_1 = 0, \quad x \in \partial\Omega. \quad (3.14)$$

The solvability condition for u_1 , obtained by the divergence theorem, determines the unknown constant u_0 as

$$u_0 = \frac{C_1}{N\bar{C}}, \quad \bar{C} \equiv \frac{1}{N} (C_1 + \dots + C_N). \quad (3.15)$$

In terms of the Neumann Green's function of (2.14), and an unknown constant χ_1 , the solution to (3.14) is

$$u_1 = 4\pi \sum_{i=1}^N (\delta_{i1} - u_0) C_i G(x; x_i) + \chi_1, \quad \chi_1 = \frac{1}{|\Omega|} \int_{\Omega} u_1 dx. \quad (3.16)$$

Next, by expanding u_1 as $x \rightarrow x_j$, and using the local behavior $G(x; x_i) \sim 1/(4\pi|x - x_i|) + R_{i,i}$ of G as $x \rightarrow x_i$ from (2.14 b), we obtain that

$$u_1 \sim \begin{cases} \frac{(1-u_0)C_1}{|x-x_1|} + A_1 + \chi_1, & \text{as } x \rightarrow x_1, \\ -\frac{u_0 C_j}{|x-x_j|} + A_j + \chi_1, & \text{as } x \rightarrow x_j, \quad j = 2, \dots, N. \end{cases} \quad (3.17 a)$$

Here, the constants A_j for $j = 1, \dots, N$ are defined by

$$A_1 = 4\pi C_1 R_{1,1} - 4\pi u_0 \left(C_1 R_{1,1} + \sum_{i=2}^N C_i G_{1,i} \right); \quad A_j = 4\pi C_1 G_{j,1} - 4\pi u_0 \left(C_j R_{j,j} + \sum_{\substack{i=1 \\ i \neq j}}^N C_i G_{j,i} \right), \quad j = 2, \dots, N. \quad (3.17 b)$$

Upon substituting (3.17) into the matching condition (3.11), we obtain that the solution w_1 to (3.10 b) must satisfy $w_1 \sim A_j + \chi_1$ as $|y| \rightarrow \infty$. Thus, $w_1 = (A_j + \chi_1)(1 - w_c)$, where w_c is the solution to (2.10 a). Upon, using the far-field behavior (2.10 b) for w_c , and substituting the resulting expression into the matching condition (3.11), we obtain that u_2 satisfies (3.8) with singularity behavior

$$u_2 \sim -\frac{C_j (A_j + \chi_1)}{|x - x_j|} + (\delta_{j1} - u_0) \frac{P_j \cdot (x - x_j)}{|x - x_j|^3}, \quad \text{as } x \rightarrow x_j, \quad j = 1, \dots, N. \quad (3.18)$$

Therefore, in terms of distributions, u_2 satisfies

$$\Delta u_2 = 4\pi \sum_{j=1}^N C_j (A_j + \chi_1) \delta(x - x_j) + 4\pi \sum_{j=1}^N (\delta_{j1} - u_0) P_j \cdot \nabla \delta(x - x_j), \quad x \in \Omega, \quad (3.19)$$

with $\partial_n u_2 = 0$ on $x \in \partial\Omega$. The solvability condition for u_2 , obtained by the divergence theorem, determines χ_1 as

$$\chi_1 = -\frac{1}{N\bar{C}} \sum_{j=1}^N A_j C_j. \quad (3.20)$$

Finally, we substitute (3.17 b) for A_j into (3.20) and write the resulting expression for χ_1 in matrix form by using the Green's matrix \mathcal{G} of (2.22). We summarize our result as follows:

Principal Result 3.2: *In the limit $\varepsilon \rightarrow 0$ of small trap radius, the splitting probability u , satisfying (3.6), is given asymptotically in the outer region $|x - x_j| \gg \mathcal{O}(\varepsilon)$ for $j = 1, \dots, N$ by*

$$u \sim \frac{C_1}{N\bar{C}} + 4\pi\varepsilon C_1 \left[G(x; x_1) - \frac{1}{N\bar{C}} \sum_{j=1}^N C_j G(x; x_j) \right] + \varepsilon\chi_1 + \mathcal{O}(\varepsilon^2), \quad (3.21 a)$$

where χ_1 is given by

$$\chi_1 = -\frac{4\pi C_1}{N\bar{C}} \left[(\mathcal{G}\mathbf{c})_1 - \frac{1}{N\bar{C}} \mathbf{c}^T \mathcal{G}\mathbf{c} \right]. \quad (3.21 b)$$

Here \mathcal{G} is the Green's matrix of (2.22), $\mathbf{c} = (C_1, \dots, C_N)^T$, and $(\mathcal{G}\mathbf{c})_1$ is the first component of $\mathcal{G}\mathbf{c}$. The averaged splitting probability $\bar{u} \equiv |\Omega|^{-1} \int_{\Omega} u dx$, which assumes a uniform distribution of starting points $x \in \Omega$, is

$$\bar{u} \sim \frac{C_1}{N\bar{C}} + \varepsilon\chi_1 + \mathcal{O}(\varepsilon^2). \quad (3.21 c)$$

From (3.21 a) we observe that $u \sim C_1/(N\bar{C})$, so that there is no leading-order effect on the splitting probability u of either the location of the source, the target, or the surrounding traps. If $C_j = 1$ for $j = 1, \dots, N$, then $u \sim 1/N$. Therefore, for this equal-capacitance case, then to leading-order in ε it is equally likely to reach any one of the N possible traps. If the target at x_1 has a larger capacitance C_1 than those of the other traps at x_j for $j = 2, \dots, N$, then the leading order theory predicts that $u > 1/N$. The formulae for the capacitances in Table 1 can be used to calculate the leading order term for u for different shapes of either the target or surrounding traps.

Next, we use (3.21) to illustrate the more interesting effect on u of the relative locations of the source, target, and surrounding traps. In the two examples below, Ω is taken to be the unit sphere, for which the Green's function and its regular part, as required in (3.21), are given analytically in (2.26 a) and (2.26 b), respectively.

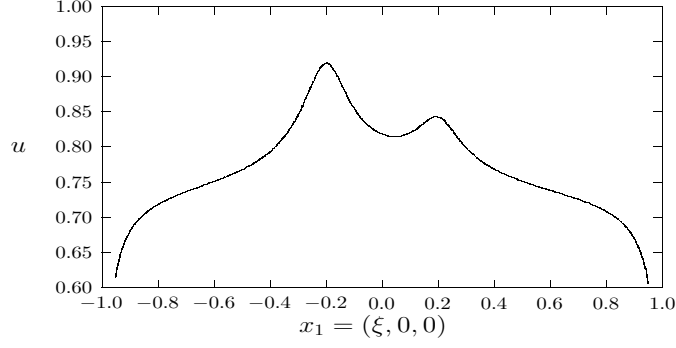
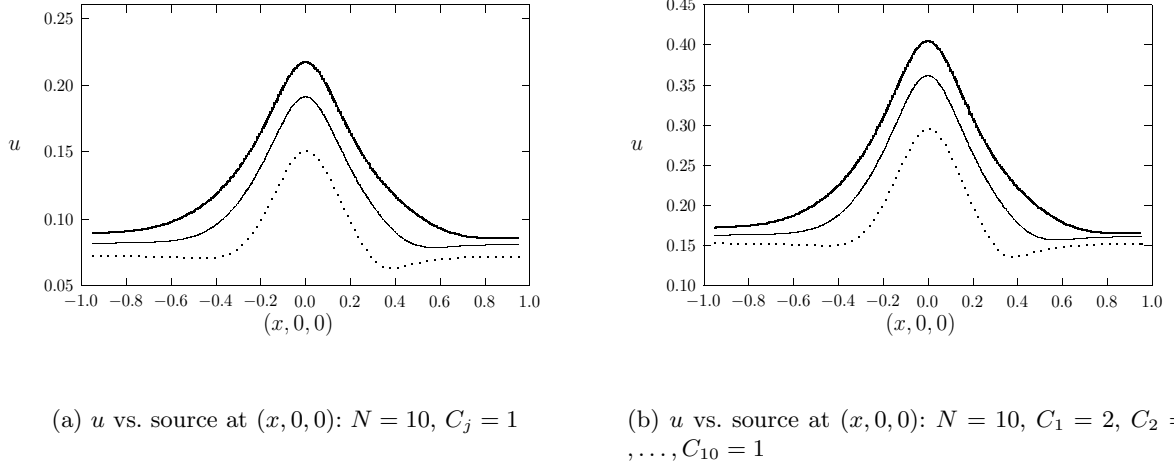


FIGURE 4. Left figure: the splitting probability u , computed from (3.22), versus the location $x_1 = (\xi, 0, 0)$ of the center of a target sphere of radius 1.5ϵ . The other trap centered at $x_2 = (0.2, 0.08, 0.0)$ is a sphere of radius 0.5ϵ . Here $\epsilon = 0.04$ and the source is at $x = (-0.2, 0.08, 0)$.



(a) u vs. source at $(x, 0, 0)$: $N = 10$, $C_j = 1$

(b) u vs. source at $(x, 0, 0)$: $N = 10$, $C_1 = 2$, $C_2 = \dots, C_{10} = 1$

FIGURE 5. Left figure: the splitting probability u versus the location $x = (x, 0, 0)$ of the source for a target trap centered at $x_1 = (0, 0, 0.2)$ surrounded by nine traps centered at optimally spaced points on an inner sphere that is concentric with the unit sphere. The inner sphere has radius $r_s = 0.7$ (heavy solid curve), $r_s = 0.5$ (solid curve), or $r_s = 0.35$ (dashed curve). The target and surrounding traps are spheres of a common radius $\epsilon = 0.04$ so that $C_j = 1$ for $j = 1, \dots, 10$. Right figure: same spatial configuration of traps with $\epsilon = 0.04$ except that the target sphere has twice the capacitance of the surrounding traps, i.e. $C_1 = 2$ and $C_j = 1$ for $j = 2, \dots, 10$.

We first consider the two-trap case $N = 2$. Then, (3.21) is readily reduced to

$$u \sim \frac{C_1}{C_1 + C_2} + 4\pi\epsilon C_1 \left(\frac{C_2}{C_1 + C_2} (G_1 - G_2) - \frac{1}{(C_1 + C_2)^2} [C_2 (C_1 R_{11} - C_2 R_{22}) + C_2 (C_2 - C_1) G_{12}] \right). \quad (3.22)$$

Here we have defined $G_1 \equiv G_1(x; x_1)$, $G_2 \equiv G_2(x; x_1)$, $G_{12} \equiv G_1(x_1; x_2)$, $R_{11} \equiv R(x_1; x_1)$, and $R_{22} \equiv R(x_2; x_2)$. We first consider the specific example in [4] corresponding to a target centered at a variable point $x_1 = (\xi, 0, 0)$, a trap centered at $x_2 = (0.2, 0.08, 0.0)$, and a fixed source location at $x = (-0.2, 0.08, 0)$. The target is a sphere of radius 1.5ϵ , while the other trap is a sphere of radius 0.5ϵ , where $\epsilon = 0.04$. Thus, $C_1 = 1.5$ and $C_2 = 0.5$. The

No. of Traps		Spherical Coordinates of Optimal Trap Locations										
9	θ	0.000	1.207	1.207	1.325	1.325	1.561	2.361	2.415	2.415		
	ϕ	0.000	0.000	2.369	3.639	5.013	1.185	4.326	2.369	0.000		

Table 3. Spherical coordinates (θ, ϕ) of the optimal locations of nine traps on the boundary of a sphere.

probability u of first reaching the target trap at $x_1 = (\xi, 0, 0)$, with $-1 < \xi < 1$, is shown in Fig. 4, and agrees with Fig. 12(b) of [4]. The notable qualitative feature in Fig. 4 of u having two local maxima is discussed in [4]. The leading order theory predicts that $u \sim C_1/(C_1 + C_2) = 3/4$, but the higher-order in ε effect of the spatial configuration of target, trap, and source, as seen in Fig. 4, is clearly significant even at $\varepsilon = 0.04$.

For the special case of two small spherical traps of radii εa_1 and εa_2 centered at $x_1 \in \Omega$ and $x_2 \in \Omega$, respectively, an approximation for the splitting probability was derived in equation (64) of [4] by using a pseudo-Green's function technique. In terms of our notation, this result of [4] can be written as

$$u(x) \sim \frac{G(x; x_1) - G(x; x_2) + (4\pi\varepsilon a_2)^{-1} + R_{22} - G_{12}}{(4\pi\varepsilon a_1)^{-1} + (4\pi\varepsilon a_2)^{-1} + R_{11} + R_{22} - 2G_{12}}. \quad (3.23)$$

By rewriting (3.23) as

$$u(x) \sim \frac{a_1 + 4\pi\varepsilon a_2 a_1 [G(x; x_1) - G(x; x_2) + R_{22} - G_{12}]}{a_1 + a_2 + 4\pi\varepsilon (a_1 a_2) (R_{11} + R_{22} - 2G_{12})}, \quad (3.24)$$

and expanding (3.24) for $\varepsilon \rightarrow 0$, we recover the two-term expansion (3.22), provided that we correctly identify $a_1 = C_1$ and $a_2 = C_2$. Therefore, for the case of two spherical targets, (3.22) agrees with equation (64) of [4] through terms of order $\mathcal{O}(\varepsilon)$.

Next, we consider a nontrivial example of (3.21) for $N = 10$ traps that has an interesting qualitative interpretation. We take a target trap centered near the origin at $x_1 = (0, 0, 0.2)$ and surround it with 9 traps with centers optimally spaced on an inner sphere that is concentric with the unit disk Ω . The spherical angular coordinates of these points are given in Table 3, and were computed numerically by the method of §2.2. The inner sphere is taken to have a radius of either $r_s = 0.7$, $r_s = 0.5$, or $r_s = 0.35$. The target and surrounding traps are spheres with a common radius $\varepsilon = 0.04$, so that $C_j = 1$ for $j = 1, \dots, 10$. In Fig. 5(a) we plot u , computed from (3.21), for a source position on the x -axis at location $(x, 0, 0)$ with $-1 < x < 1$. For these parameter values, the leading order theory predicts that $u \sim 0.1$. From Fig. 5(a) we observe a clear screening effect. When the source is outside the inner sphere, which effectively acts as a “wall” of traps, it is difficult to reach the target sphere centered at $(0, 0, 0.2)$. Therefore, when the source is outside the inner sphere we would expect $u < 0.1$. This is clearly observed in Fig. 5(a). However, we would expect that u increases considerably when the source crosses inside the inner sphere, as the target sphere near the origin is then well-isolated from the surrounding traps and is in closer proximity to the source. If the inner sphere has a smaller radius, such as $r_s = 0.35$, then the target sphere is not as isolated from the surrounding traps as when $r_s = 0.7$. Correspondingly, the peak in u is not as pronounced near the origin when $r_s = 0.35$ as it is for larger values of r_s . This is precisely what is observed in Fig. 5(a). The local minimum in u in the dashed curve of Fig. 5(a) for a source point at $(x, 0, 0) \approx (0.35, 0, 0)$ is due to a nearby trap on the inner

sphere centered at $x_2 \approx (0.327, 0.0, 0.125)$. This nearby trap significantly lowers the probability that the target near the origin will be reached first. In Fig. 5(b) we show the corresponding result for the case when the target trap centered at $x_1 = (0, 0, 2)$ has a higher capacitance of $C_1 = 2$ relative to the surrounding traps on the inner sphere with $C_j = 1$ for $j = 2, \dots, 10$. To leading order in ε , we expect $u \sim 2/11 \approx 0.182$. For this case, we observe from Fig. 5(b) a weaker screening effect together with a more pronounced peak in u near the origin, as expected intuitively.

There are many other qualitatively interesting applications of Principal Result 3.2 for different arrangements of a target and surrounding traps. However, we emphasize that (3.21) applies only in the outer region $|x - x_j| \gg \mathcal{O}(\varepsilon)$ and for $|x_i - x_j| \gg \mathcal{O}(\varepsilon)$. Thus, the source and traps must be well-separated, and no two traps can be closely spaced by $\mathcal{O}(\varepsilon)$. For two closely-spaced, but non-overlapping, spherical traps of the same radius, one can use (2.25) for the capacitance of the two-sphere cluster and then modify (3.21) accordingly. The details are left to the reader.

4 Conclusion

The method of matched asymptotic expansions was used to calculate a two-term asymptotic expansion for the principal eigenvalue of the Laplacian in a three-dimensional domain with a reflecting boundary that contains N interior traps of asymptotically small radii. The coefficient of the second-order term in this asymptotic expansion was found to depend on the locations of the traps within the domain. The principal eigenvalue is inversely proportional to the average mean first passage time for the capture of a Brownian particle within the domain. For small values of N , numerical methods of global optimization were used to determine the spatial configuration of spherical traps of small radii within the unit sphere that maximize the principal eigenvalue, or correspondingly minimize the average mean first passage time for capture. A related problem of the asymptotic calculation of the splitting probability in a three-dimensional domain with localized traps was also investigated, and illustrated for a spherical domain.

There are a few open problems that warrant further study. The first open problem is to give a rigorous justification of the two-term asymptotic result for the asymptotic expansion of the principal eigenvalue in Principal Result 2.1 and for the splitting probability in Principal Result 3.2. The second open problem is to determine, for large values of N , the spatial configuration $\{x_1, \dots, x_N\}$ of the centers of N interior spherical traps of a common radius ε that maximize the coefficient of the $\mathcal{O}(\varepsilon^2)$ term in the asymptotic expansion of the principal eigenvalue in Principal Result 2.1. For $2 \leq N \leq 20$ the optimal arrangements were computed in §2.2. For $N \rightarrow \infty$, but in the limit of small trap volume fraction $N\varepsilon^3 \ll 1$, we would like to derive a scaling law associated with this optimal arrangement, and to explore whether such a result could be derived from techniques of homogenization theory. A third open problem is to consider the optimization of the principal eigenvalue in non-spherical domains with N localized traps. In particular, for the unit cube, the periodic Green's function, as given explicitly in [19], can be adapted for use in Principal Result 2.1.

Acknowledgements

A. F. C. and M. J. W. both gratefully acknowledge the grant support of NSERC (Canada). We also thank Sheldon Richards and Prof. Raymond Spiteri of the U. Saskatchewan for independently verifying our computational results reported in Table 2 for the optimal configuration of traps within a sphere by using the Lipschitz-Continuous Global Optimization (LGO) method of [24]. M. J. W. is also grateful to Prof. O. Benichou for an interesting correspondence regarding the comparison of our results for the splitting probability with that obtained in [4] for the case of two spherical traps.

Appendix A The Neumann Green's Function for the Sphere

We now calculate the Neumann Green's function $G(x, \xi)$ satisfying (2.14) when Ω is a sphere of radius a for which $|\Omega| = 4\pi a^3/3$. We decompose G and introduce ϕ by

$$G(x; \xi) = \frac{1}{4\pi|x - \xi|} + \frac{1}{6|\Omega|} (|x|^2 + |\xi|^2) + \frac{1}{4\pi}\phi(x; \xi). \quad (\text{A.1})$$

Upon substituting (A.1) into (2.14), we find that ϕ satisfies

$$\Delta\phi = 0, \quad x \in \Omega; \quad \partial_n\phi = -\frac{1}{a^2} - \partial_n \left(\frac{1}{|x - \xi|} \right), \quad x \in \partial\Omega. \quad (\text{A.2})$$

To solve (A.2) we choose a coordinate system so that the source point $x = \xi$ is on the positive z axis. Then, since $\Delta\phi = 0$ and ϕ is axisymmetric, then ϕ admits the series expansion

$$\phi(x; \xi) = \sum_{n=0}^{\infty} B_n P_n(\cos\theta) \left(\frac{|x||\xi|}{a^2} \right)^n. \quad (\text{A.3})$$

Here $P_n(z)$ is the Legendre polynomial of integer n and the B_n for $n = 0, 1, \dots$ are coefficients to be determined. Notice that we have enforced that $\phi(x; \xi) = \phi(\xi; x)$ so that $G(x; \xi) = G(\xi; x)$. The coefficients B_n in (A.3) are determined upon satisfying the boundary conditions in (A.2). We let $\rho = |x|$ and calculate that

$$\partial_n\phi|_{\partial\Omega} = \partial_\rho\phi|_{\rho=a} = \sum_{n=0}^{\infty} \frac{nB_n}{a^{n+1}} P_n(\cos\theta) |\xi|^n. \quad (\text{A.4})$$

Next, we recall the generating function for Legendre polynomials given by

$$\frac{1}{\sqrt{1 - 2tz + t^2}} = \sum_{k=0}^{\infty} t^k P_k(z), \quad |t| < \min|z \pm \sqrt{z^2 - 1}|. \quad (\text{A.5})$$

We let $z = \cos\theta$ and $t = |\xi|/|x|$ so that

$$\frac{1}{|x - \xi|} = \frac{1}{\sqrt{|\xi|^2 - 2|x||\xi|\cos\theta + |x|^2}} = \sum_{n=0}^{\infty} \frac{|\xi|^n}{|x|^{n+1}} P_n(\cos\theta). \quad (\text{A.6})$$

By differentiating this expression with respect to $|x|$ we get

$$\partial_\rho (|x - \xi|^{-1})|_{\rho=a} = - \sum_{n=0}^{\infty} \frac{(n+1)|\xi|^n}{a^{n+2}} P_n(\cos\theta). \quad (\text{A.7})$$

Upon substituting (A.4) and (A.7) into the boundary condition given in (A.2), we obtain

$$\sum_{n=0}^{\infty} \left(nB_n - \frac{(n+1)}{a} \right) P_n(\cos \theta) \frac{|\xi|^n}{a^{n+1}} = -\frac{1}{a^2}. \quad (\text{A.8})$$

Since B_0 is arbitrary, we can choose $B_0 = 1/a$ for convenience below. The other coefficients must satisfy

$$B_n = \frac{1}{a} + \frac{1}{na}, \quad \text{for } n \geq 1; \quad B_0 = \frac{1}{a}. \quad (\text{A.9})$$

Upon substituting (A.9) into (A.3), we can represent ϕ in terms of two infinite series as

$$\phi(x; \xi) = \frac{1}{a} \sum_{n=0}^{\infty} P_n(\cos \theta) \left(\frac{|x||\xi|}{a^2} \right)^n + \frac{1}{a} \sum_{n=1}^{\infty} \frac{1}{n} P_n(\cos \theta) \left(\frac{|x||\xi|}{a^2} \right)^n. \quad (\text{A.10})$$

The first infinite sum in (A.10) is readily summed by using the generating function (A.5) to get

$$\frac{1}{a} \sum_{n=0}^{\infty} P_n(\cos \theta) \left(\frac{|x||\xi|}{a^2} \right)^n = \frac{a}{|x|r'}, \quad (\text{A.11})$$

where $x' = xa^2/|x|^2$ is the image point to x outside the sphere and $r' \equiv |x' - \xi|$. To calculate the second infinite sum in (A.10), we begin by defining $I(\beta)$ by

$$I(\beta) = \sum_{n=1}^{\infty} \frac{1}{n} P_n(\cos \theta) \beta^n. \quad (\text{A.12})$$

Upon differentiating (A.12) and then using the generating function (A.5) we get

$$I'(\beta) = \frac{-1}{\beta} \left[1 - \sum_{n=0}^{\infty} P_n(\cos \theta) \beta^n \right] = \frac{1}{\beta} \left[\frac{1}{\sqrt{\beta^2 - 2\beta \cos \theta + 1}} - 1 \right]. \quad (\text{A.13})$$

Since $I(0) = 0$, then $I(\beta)$ can be expressed as a definite integral that is readily evaluated as (cf. page 95 of [9])

$$I(\beta) = \int_0^\beta \frac{1}{s} \left[\frac{1}{\sqrt{s^2 - 2s \cos \theta + 1}} - 1 \right] ds = \log \left(\frac{2}{1 - \beta \cos \theta + \sqrt{1 + \beta^2 - 2\beta \cos \theta}} \right). \quad (\text{A.14})$$

The second infinite sum in (A.10) is simply $a^{-1}I(\beta)$ where $\beta = |x||\xi|/a^2$. By using the resulting expression, together with (A.11), to replace the two infinite sums in (A.10), we obtain after a short calculation that

$$\phi(x; \xi) = \frac{a}{|x|r'} + \frac{1}{a} \log \left(\frac{2a^2}{a^2 - |x||\xi| \cos \theta + |x|r'} \right), \quad x' = \frac{a^2 x}{|x|^2}, \quad r' = |x' - \xi|. \quad (\text{A.15})$$

Finally, we substitute (A.15) into (A.1) to obtain an explicit expression for G up to a constant B ,

$$G(x; \xi) = \frac{1}{4\pi|x - \xi|} + \frac{a}{4\pi|x|r'} + \frac{1}{4\pi a} \log \left(\frac{2a^2}{a^2 - |x||\xi| \cos \theta + |x|r'} \right) + \frac{1}{6|\Omega|} (|x|^2 + |\xi|^2) + B. \quad (\text{A.16})$$

The constant B is to be chosen so that $\int_{\Omega} G(x; \xi) dx = 0$. The following lemma proves that B is independent of ξ .

Lemma A.1 *Suppose that $G(x; \xi)$ satisfies*

$$\Delta G = \frac{1}{|\Omega|} - \delta(x - \xi), \quad x \in \Omega; \quad \partial_n G = 0, \quad x \in \partial\Omega, \quad (\text{A.17})$$

with $G(x; \xi) = G(\xi; x)$. Then, $\int_{\Omega} G(x; \xi) dx$ is a constant independent of ξ .

To prove this simple result we calculate as follows:

$$0 = \int_{\Omega} G(x; \xi') \left[\Delta G(x; \xi) - \frac{1}{|\Omega|} + \delta(x - \xi) \right] dx = G(\xi; \xi') - \frac{1}{|\Omega|} \int_{\Omega} G(x; \xi') dx + \int_{\Omega} G(x; \xi') \Delta G(x; \xi) dx,$$

$$0 = G(\xi; \xi') - \frac{1}{|\Omega|} \int_{\Omega} G(x; \xi') dx + \int_{\Omega} \nabla \cdot [G(x; \xi') G(x; \xi)] dx - \int_{\Omega} \nabla G(x; \xi) \cdot \nabla G(x; \xi') dx.$$

Then, upon using the divergence theorem and the boundary condition $\partial_n G = 0$ on $\partial\Omega$, we conclude that

$$\frac{1}{|\Omega|} \int_{\Omega} G(x; \xi') dx = G(\xi; \xi') - \int_{\Omega} \nabla G(x; \xi) \cdot \nabla G(x; \xi') dx. \quad (\text{A.18})$$

Since the right-hand side of (A.18) is symmetric in ξ and ξ' it follows that $\int_{\Omega} G(x; \xi') dx = \int_{\Omega} G(x; \xi) dx$. ■

Since B in (A.16) is independent of ξ , we can conveniently calculate this constant by setting $\int_{\Omega} G(x; 0) dx = 0$. Setting $\xi = 0$ in (A.16), using the radial symmetry of $G(x; 0)$, and noting that $r' = a^2/\rho$ with $\rho = |x|$, we obtain that the condition $\int_{\Omega} G(x; 0) dx = 0$ becomes

$$\frac{1}{4\pi} \int_0^a \rho^2 \left(\frac{1}{\rho} + \frac{1}{a} \right) d\rho + \frac{1}{8\pi a^3} \int_0^a \rho^4 d\rho + B \int_0^a \rho^2 d\rho = 0.$$

This yields $B = -7/(10\pi a)$. Upon setting $a = 1$ we obtain the explicit formula (2.26 a) for G for the unit sphere.

References

- [1] G. Beliakov, *The Cutting Angle Method - A Tool for Constrained Global Optimization*, Optimization Methods and Software, **19**, No. 2, (2004), pp. 137–151.
- [2] O. Bénichou, R. Voituriez, *Narrow Escape Time Problem: Time Needed for a Particle to Exit a Confining Domain Through a Small Window*, Phys. Rev. Lett, **100**, (2008), 168105.
- [3] A. Cheviakov, M. J. Ward, R. Straube, *An Asymptotic Analysis of the Mean First Passage Time for Narrow Escape Problems: Part II: The Sphere*, to appear, SIAM Multiscale Modeling and Simulation, (2010), (32 pages).
- [4] S. Condamin, O. Bénichou, M. Moreau, *Random Walks and Brownian Motion: A Method of Computation for First-Passage Times and Related Quantities in Confined Geometries*, Phys. Rev. E., **75**, (2007), 021111.
- [5] D. Coombs, R. Straube, M. J. Ward, *Diffusion on a Sphere with Localized Traps: Mean First Passage Time, Eigenvalue Asymptotics, and Fekete Points*, SIAM J. Appl. Math., **70**, No. 1, (2009), pp. 302–332.
- [6] B. U. Felderhof, D. Palaniappan, *Electrostatic Capacitance of Two Unequal Overlapping Spheres and the Rate of Diffusion-Controlled Absorption*, J. Appl. Physics, **86**, No. 11, (1999), pp. 6501–6506.
- [7] M. Flucher, *Approximation of Dirichlet Eigenvalues on Domains with Small Holes*, J. Math. Anal. Appl., **193**, No. 1, (1995), pp. 169–199.
- [8] GANSO Software Library: University of Ballarat, Ballarat, Victoria, Australia; www.ballarat.edu.au/ciao.
- [9] I. M. Gradshteyn, I. M. Ryzhik, *Table of Integrals, Series, and Products*, corrected and enlarged edition, pp. 36–41, (1980) Academic Press, San Diego.
- [10] E. M. Harrell II, P. Kröger, K. Kurata, *On the Placement of an Obstacle or a Well so as to Optimize the Fundamental Eigenvalue*, SIAM J. Math. Anal., **33**, No. 1, (2001), pp. 240–259.
- [11] D. Holcman, Z. Schuss, *Escape Through a Small Opening: Receptor Trafficking in a Synaptic Membrane*, J. Stat. Phys., **117**, No. 5–6, (2004), pp. 975–1014.
- [12] D. Holcman, Z. Schuss, *Diffusion Escape Through a Cluster of Small Absorbing Windows*, J. of Phys. A: Math Theor., **41**, (2008), 155001 (15pp).
- [13] R. Horst, P. M. Pardalos (Eds.), *Handbook of Global Optimization*, Kluwer Academic Publishers, Dordrecht, Boston, (1995).
- [14] J. D. Jackson, *Classical Electrodynamics*, Wiley, New York, 2nd Edition, (1945).
- [15] O. D. Kellogg, *Foundations of Potential Theory*, Springer-Verlag, Berlin, (1967), (reprinted from the first edition of 1929).

- [16] T. Kolokolnikov, M. S. Titcombe, M. J. Ward, *Optimizing the Fundamental Neumann Eigenvalue for the Laplacian in a Domain with Small Traps*, European J. Appl. Math., **16**, No. 2, (2005), pp. 161–200.
- [17] J. D. Love, *A Note on the Capacitance of Two Closely Separated Spheres*, J. Inst. Math. Applics., **24**, (1979), pp. 255–257.
- [18] M. A. Mammadov, A. Rubinov, J. Yearwood, *Dynamical Systems Described by Relational Elasticities with Applications to Global Optimization*. In: A. Rubinov and V. Jeyakumar (Eds.), *Continuous Optimization: Current Trends and Modern Applications*, Springer, New York, (2005), pp. 365–385.
- [19] S. L. Marshall, *A Periodic Green Function for Calculation of Coulombic Lattice Potentials*, J. Phys: Condens. Matter **12**, (2000), pp. 4575–4601.
- [20] S. Ozawa, *Singular Variation of Domains and Eigenvalues of the Laplacian*, Duke Math. J., **48**, No. 4, (1981), pp. 767–778.
- [21] S. Ozawa, *An Asymptotic Formula for the Eigenvalues of the Laplacian in a Three-Dimensional Domain with a Small Hole*, J. Fac. Sci. Univ. Tokyo Sect. 1A Math., **30**, No. 2, (1983), pp. 243–257.
- [22] S. Ozawa, *Asymptotic Property of an Eigenfunction of the Laplacian under Singular Variation of Domains – the Neumann Condition*, Osaka J. Math., **22**, No. 4, (1985), pp. 639–655.
- [23] S. Pillay, M. J. Ward, A. Peirce, T. Kolokolnikov, *An Asymptotic Analysis of the Mean First Passage Time for Narrow Escape Problems: Part I: Two-Dimensional Domains*, to appear, SIAM Multiscale Modeling and Simulation, (2010), (28 pages).
- [24] J. D. Pintér, *Global Optimization in Action*, Kluwer Academic Publishers, Dordrecht, Netherlands, (1996).
- [25] S. Redner, *A Guide to First-Passage Time Processes*, Cambridge Univ. Press, (2001), Cambridge, U.K.
- [26] A. Rubinov, V. Jeyakumar (Eds.), *Continuous Optimization: Current Trends and Modern Applications*, Springer, New York, (2005).
- [27] Z. Schuss, A. Singer, D. Holcman, *The Narrow Escape Problem for Diffusion in Cellular Microdomains*, PNAS, **104**, No. 41, (2007), pp. 16098–16103.
- [28] A. Singer, Z. Schuss, D. Holcman, R. S. Eisenberg, *Narrow Escape, Part I*, J. Stat. Physics, **122**, No. 3, (2006), pp. 437–463.
- [29] A. Singer, Z. Schuss, D. Holcman, *Narrow Escape, Part II: The Circular Disk*, J. Stat. Phys., **122**, No. 3, (2006), pp. 465–489.
- [30] A. Singer, Z. Schuss, D. Holcman, *Narrow Escape, Part III: Non-Smooth Domains and Riemann Surfaces*, J. Stat. Phys., **122**, No. 3, (2006), pp. 491–509.
- [31] C. A. Swanson, *Asymptotic Variational Formulae for Eigenvalues*, Canad. Math. Bull., **6**, (1963), pp. 15–25.
- [32] G. Szegő, *Ueber Einige Extremalaufgaben der Potential Theorie*, Math. Z., **31**, (1930), p. 583–593.
- [33] A. Taffia, D. Holcman, *Dwell Time of a Brownian Molecule in a Microdomain with Traps and a Small Hole on the Boundary*, J. Chem. Phys., **126**, No. 23, (2007), 234107.
- [34] M. J. Ward, J. B. Keller, *Strong Localized Perturbations of Eigenvalue Problems*, SIAM J. Appl. Math., **53**, No. 3, (1993), pp. 770–798.
- [35] M. J. Ward, W. D. Henshaw, J. B. Keller, *Summing Logarithmic Expansions for Singularly Perturbed Eigenvalue Problems*, SIAM J. Appl. Math., **53**, No. 3, (1993), pp. 799–828.
- [36] E. Weber, *Electromagnetic Fields*, John Wiley, New York, (1950).